Design of an Interdigital Band-Pass Filter for Out-of-Band Rejection Improvement

Weiping Li[1, 2, *], Xin Cao[1], Haodong Lin[1], and Zong-Xi Tang[1]

Abstract—In this letter, an interdigital band-pass filter is proposed for out-of-band rejection improvement. Seven quarter-wavelength resonators are employed to form the passband. Three extra transmission zeros (TZs) on both sides of the passband are implemented by introducing source-load coupling and dumbbell defected ground structures (DGS). As demonstrated by the measured results, out-of-band rejection and selectivity are improved by these three TZs, and good performances are achieved. The proposed method of increasing out-of-band rejection is feasible and applicable in the design of modern microstrip filters.

1. INTRODUCTION

With the rapid development of modern wireless communication technology, microwave filters are an indispensable part of the communication systems for signal selection. Filters with good performance, satisfactory specifications, compact size and low cost have attracted many researchers' attention and become a hot research area [1–3]. One major concern for the performance of microstrip band-pass filters is out-of-band rejection. An effective way to enhance out-of-band rejection is to create transmission zeros (TZs) beside the passbands [4, 5]. For filters with multiple resonators, one direct way to create TZs is cross-coupling. This method can produce one or two TZs on either side of the passbands, and it has been widely applied in cavity filters. However, one disadvantage of cross-coupling method is that the positions where the TZs appear are related to the coupling matrix, which suggests that the TZs are not independent from the passbands of the filters [6, 7]. Moreover, it is difficult to apply this method to the resonators with irregular geometric topologies [8]. To solve this problem, source-load coupling and dumbbell DGSs are applied in the proposed filter to create TZs. The filter is simulated and fabricated. As demonstrated by the measured results, three flexible TZs have been produced and excellent performances have been achieved.

2. THEORY AND DESIGN PROCESS

The topology of a microstrip quarter-wavelength is shown in Fig. 1. It consists of a microstrip line with one end open and the other end shorted to the ground through a metallic via hole.

This resonator can be regarded as a short-circuited transmission line of length $\lambda/4$. The input impedance of a shorted line of length l is [9]

$$Z_{in} = Z_0 \tanh\left(\alpha + j\beta\right) l = Z_0 \frac{\tanh\alpha l + j\tan\beta l}{1 + j\tan\beta l\tanh\alpha l} = Z_0 \frac{1 - j\tanh\alpha l\cot\beta l}{\tanh\alpha l - j\cot\beta l} \tag{1}$$

Figure 1. The topology of a quarter-wavelength resonator.

where α and β are the attenuation constant and phase constant, respectively. Now assume that $l = \lambda/4$ at $\omega = \omega_0$, and let $\omega = \omega_0 + \Delta\omega$. Then, for a quasi-TEM line,

$$\beta l = \frac{\omega_0 l}{v_p} + \frac{\Delta\omega l}{v_p} = \frac{\pi}{2} + \frac{\pi\Delta\omega}{2\omega_0} \tag{2}$$

where v_p is the phase velocity, so

$$\cot \beta l = \cot\left(\frac{\pi}{2} + \frac{\pi\Delta\omega}{2\omega_0}\right) = -\tan\frac{\pi\Delta\omega}{2\omega_0} \simeq \frac{-\pi\Delta\omega}{2\omega_0} \tag{3}$$

Also,

$$\tanh \alpha l \simeq \alpha l \tag{4}$$

if the dielectric loss of the substrate is small. Then, Equation (1) can be further expressed as

$$Z_{in} = Z_0 \frac{1 + j\alpha l\pi\Delta\omega/2\omega_0}{\alpha l + j\pi\Delta\omega/2\omega_0} \simeq \frac{Z_0}{\alpha l + j\pi\Delta\omega/2\omega_0} \tag{5}$$

since

$$\alpha l\pi\Delta\omega/2\omega_0 \ll 1 \tag{6}$$

And the unloaded quality factor Q_0 of the quarter-wavelength resonator can be obtained as

$$Q_0 = \frac{\pi}{4\alpha l} = \frac{\beta}{2\alpha} \tag{7}$$

at the resonance condition $l = \pi/2\beta$. Therefore, the resonant frequency and unloaded quality factor of the quarter-wavelength resonator can be determined. The next step is to calculate the coupling coefficients. Based on the low-pass filter prototype, the coupling coefficient can be given as

$$M_n = Y_A\left(\frac{J_{n,n+1}}{Y_A}\sqrt{h} + 1\right) \tag{8}$$

where $J_{n,n+1}$ is the n-th J-inverter; Y_A is the admittance of the resonator; h is the filter ratio constant. And $J_{n,n+1}$ can be expressed as

$$J_{n,n+1} = \frac{Y_A}{\sqrt{g_n g_{n+1}\omega'}} \tag{9}$$

where ω' is the normalized frequency and g_n the filter component value.

Based on the filter design guide [10], the filter component values of a seven-stage bandpass filter with Chebyshev response can be given as: $g_0 = g_8 = 1$, $g_1 = g_7 = 0.93$, $g_2 = g_6 = 1.43$, $g_3 = g_5 = 1.87$, and $g_4 = 1.63$. The center frequency of the filter is designed to be 1.65 GHz. The substrate is Arlon AD 1000 with comparative dielectric constant $\varepsilon_r = 10.2$, thickness $h = 0.762$ mm and loss tangent $\tan\delta = 0.003$. The topology of the interdigital filter is shown in Fig. 2. The resonators are placed on the substrate with their centers aligned. Based on the above equations, after tuning and optimization using the EM simulation software HFSS, the geometric parameters can be finally given as: $L_1 = 18.65$ mm, $L_2 = 17$ mm, $L_3 = 17.2$ mm, $L_4 = 17$ mm, $W_{s1} = 0.56$ mm, $W_{s2} = 0.8$ mm, $W_{s3} = 0.9$ mm, $W = 1.1$ mm and $W_{\_tap} = 7$ mm. The impedance of the input and output feed lines is $50\,\Omega$, and then W_0 can be calculated to be 0.94 mm. The diameter of the via hole is 0.5 mm.

The simulated and measured results of the interdigital filter are shown in Fig. 3. The in-band insertion loss is less than 2 dB and return loss more than 12 dB. The simulation and measurement are generally in good agreement. Due to cross couplings between the nonadjacent resonators [11], one transmission zero (TZ) is created at the right side of the passband at 1.95 GHz, resulting in a higher selectivity on that side. It can be observed form Fig. 3 that the selectivity at the left side of the
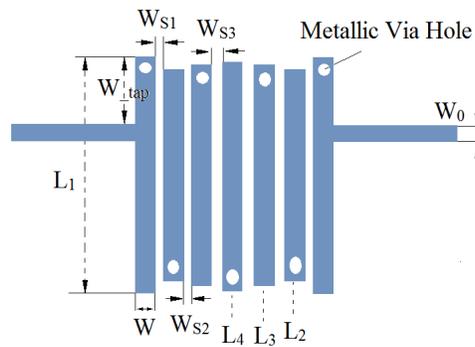
Figure 2. The topology of the interdigital filter.
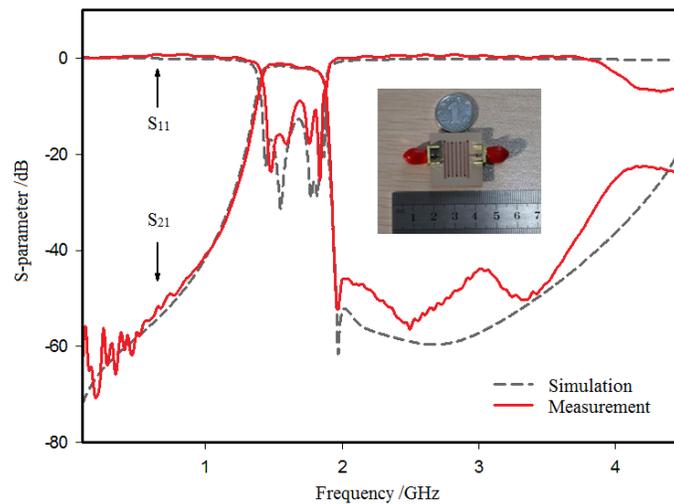
Figure 3. The simulated and measured results of the microstrip interdigital filter.

passband is not good enough, and the stopband rejection is running down from 3 GHz to 4 GHz. In order to further improve the corresponding performances of the filter, source-load coupling is employed.

As shown in Fig. 4, a bypass is added and coupled to the input and output feed lines, so the coupling between source and load is created. With the help of source-load coupling, a pair of TZs on both sides of passband can be obtained [12, 13]. In Fig. 4, $W_{\_SL}$ and $L_{\_SL}$ are used to control the coupling strength. As for the bypass, it can also work as a half-wavelength resonator, and therefore L_0 is employed to avoid this additional resonance in the transition band and stopband of the main path.

The simulated and measured results of the interdigital filter with source-load coupling are shown in Fig. 5. By comparing to the results in Fig. 3, it can be found that two extra TZs located at 1.35 GHz and 3.25 GHz are obtained with the introduction of source-load coupling. The TZ located at 1.35 GHz is near the left side of the passband, resulting in a much steeper transition band, so the selectivity is improved. The TZ located at 3.25 GHz is in the stopband, making the stopband rejection much deeper. It can be found in Fig. 5 that the rejection is more than 40 dB from 3 GHz to 4 GHz, which is better than that of Fig. 3. Especially at 3.25 GHz, the out-of-band rejection is improved over 30 dB.

Again, to further improve the performance and create another TZ without increasing the size of the filter, a dumbbell DGS is employed (as shown in Fig. 6). While the top layer remains the same, the bottom metal layer is etched into an "H" shape. This structure can prevent electromagnetic waves from propagation in the transmission line at a certain frequency point, thus a TZ can be created. If the TZ is designed properly, it can be employed to increase the out-of-band rejection in filters. The equivalent circuit of the DGS is shown in Fig. 7. The elements L_d and C_d can be calculated based on
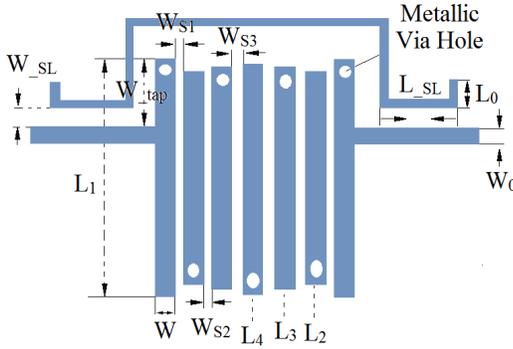
Figure 4. The topology of the interdigital filter with source-load coupling.
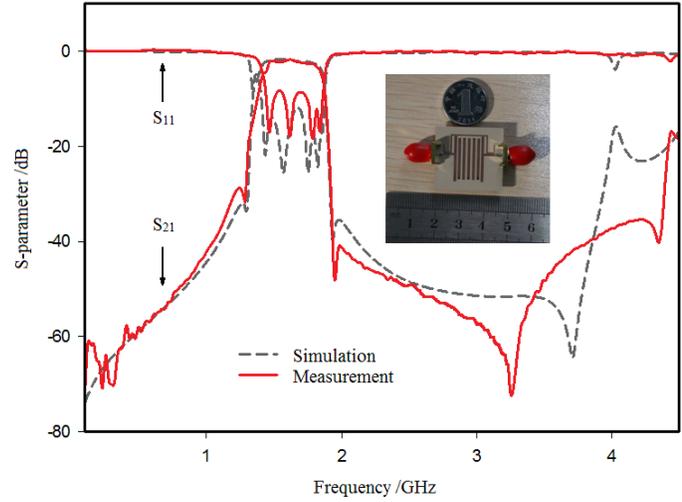
Figure 5. The simulated and measured results of the interdigital filter with source-load coupling.
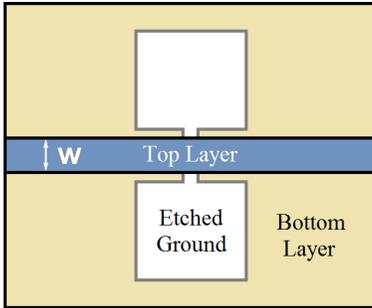
Figure 6. The structure of the DGS.
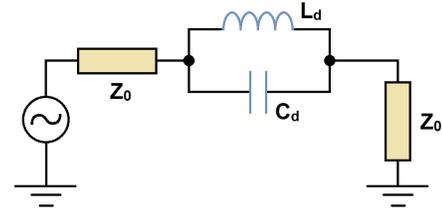
Figure 7. The equivalent circuit of the DGS.

the empirical equations as [14, 15]

$$C_d = \frac{5f_c}{\pi \left(f_0^2 - f_c^2\right)} \tag{10}$$

$$L_d = \frac{250}{\pi^2 f_0^2 C} \tag{11}$$

where f_c and f_0 are the cutoff frequency and resonant frequency of the stopband, respectively.

The topology of the filter with DGS is shown in Fig. 8. W_1, W_2 and d are used to control L_d and C_d of the DGS. Therefore, the new TZ is much more flexible. The simulation and measurement are accomplished by HFSS and Rohde & Schwarz's ZVA40 vector network analyzer, respectively. Fig. 9 depicts the simulated and measured results, which show good agreement. The topology of the proposed filter is planar and with a compact size of $0.29\lambda g \times 0.26\lambda g$, where λg is the guided wavelength of the electromagnetic waves in the substrate at the resonant frequency. The passband is centered at 1.65 GHz, with fractional bandwidth of 15.4%. The insertion loss, including SMA connector loss, is measured to be 1.6 dB, and the in-band return loss is better than 15 dB. Due to the TZs located at 1.35 GHz, 1.95 GHz, which are near the edges of the passband, sharp attenuation shirts of the passbands can be achieved. Another two TZs located at 3.25 GHz and 3.92 GHz are in the stopband, causing the rejection deeper than 50 dB from 3 GHz to 4 GHz. By comparing to the results in Fig. 5, it is obvious that the stopband rejection has been bettered, due to the extra TZ at 3.92 GHz brought by the DGS. Compared with
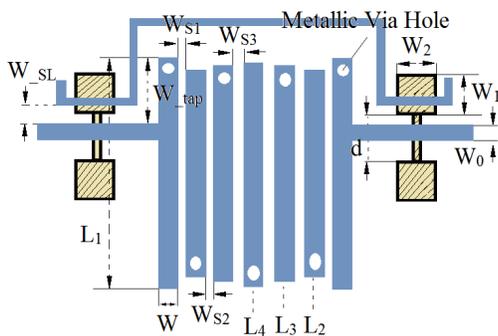
Figure 8. The topology of the filter with source-load coupling and DGS.
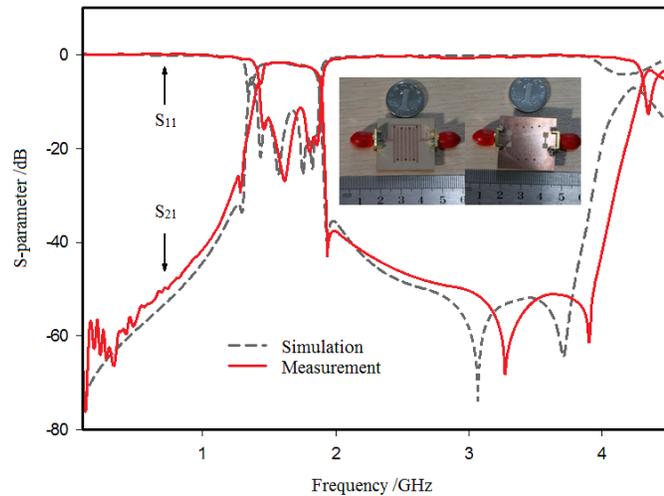
Figure 9. The simulated and measured results of the filter with source-load coupling and DGS.

the original filter depicted in Fig. 2, the out-of band rejection and selectivity are greatly improved by employing source-load coupling and DGS without major increase of size of the filter. The differences between simulation and measurement are mainly due to fabrication inaccuracy.

3. CONCLUSION

In this paper, an interdigital band-pass filter is proposed for out-of-band rejection improvement. Source-load coupling and DGS are employed to create three different TZs which improve out-of-band rejection and selectivity of the original filter without major influence on the passband. The simulated and measured results are in good agreement. The excellent performance, planar structure and compact size make the proposed filter attractive for the design of modern microwave circuits and wireless communication systems.

REFERENCES

1. Lai, Z., Z. Tang, X. Zhan, et al., "Compact multi-band transversal bandpass filters with source-load coupling," *Journal of Electromagnetic Waves and Applications*, Vol. 28, No. 2, 184–193, 2014.
2. Jankovic, N., V. Radonic, V. Crnojevic-Bengin, et al., "A compact dual-band bandpass filter using folded quarter-wavelength resonators," *2012 42nd European Microwave Conference (EuMC), IEEE*, 360–363, 2012.
3. Jankovic, N., V. Radonic, and V. Crnojevic-Bengin, "Compact tri-band bandpass filter based on quarter-wavelength resonators," *Journal of Electromagnetic Waves and Applications*, Vol. 27, No. 6, 750–757, 2013.
4. Yang, Z., L. Zhang, Z. Ma, et al., "Design of a compact dual-band dual-mode microstrip filter with an adjustable transmission zero," *2012 IEEE MTT-S International Microwave Symposium Digest (MTT), IEEE*, 1–3, 2012.

5. Wang, L., C. Zhao, C. Li, et al., "Dual-band bandpass filter using stub loaded resonators with multiple transmission zeros," *2010 9th International Symposium on Antennas Propagation and EM Theory (ISAPE), IEEE*, 1208–1211, 2010.

6. Cameron, R. J., "Advanced coupling matrix synthesis techniques for microwave filters," *IEEE Transactions on Microwave Theory and Techniques*, Vol. 51, No. 1, 1–10, 2003.

7. Zhou, M., X. Tang, and F. Xiao, "Compact dual band bandpass filter using novel E-type resonators with controllable bandwidths," *Microwave and Wireless Components Letters, IEEE*, Vol. 18, No. 12, 779–781, 2008.

8. Sun, S., L. Zhu, and H. H. Tan, "A compact wideband bandpass filter using transversal resonator and asymmetrical interdigital coupled lines," *Microwave and Wireless Components Letters, IEEE*, Vol. 18, No. 3, 173–175, 2008.

9. Pozar, D. M., *Microwave Engineering*, 4th Edition, John Wiley & Sons Inc., USA, 2012.

10. Cameron, R. J., C. M. Kudsia, and R. R. Mansour, *Microwave Filters for Communication Systems: Fundamentals, Design, and Applications*, John Wiley & Sons Inc., USA, 2007.

11. Hong, J.-S. and M. J. Lancaster, *Microstrip Filters for RF/Microwave Applications*, John Wiley & Sons Inc., USA, 2001.

12. Montejo-Garai, J. R., "Synthesis of N-even order symmetric filters with N transmission zeros by means of source-load cross coupling," *Electronics Letters*, Vol. 36, No. 3, 232–233, 2000.

13. Amari, S., "Direct synthesis of folded symmetric resonator filters with source-load coupling," *IEEE Microwave & Wireless Components Letters*, Vol. 11, No. 6, 264–266, 2001.

14. Boutejdar, A., A. Omar, M. Al Sharkawy, et al., "A simple transformation of improved WLAN band pass to low pass filter using defected ground structure (DGS), defected microstrip structure (DMS) and multilayer-technique," *Journal of Microwaves, Optoelectronics and Electromagnetic Applications*, Vol. 12, No. 1, 111–130, 2013.

15. Khan, M. T., M. A. Zakariya, M. N. M. Saad, et al., "Tuning of end-coupled line bandpass filter for 2.4 GHz using defected ground structure (DGS) parameters," *Business Engineering and Industrial Applications Colloquium (BEIAC), 2013 IEEE*, 131–134, 2013.